Publications

3-17-2022

Using Machine Learning in Estimating Changing Bed Shear over a Flume Test Box

Ghada S. Ellithy
Embry-Riddle Aeronautical University, ellithyg@erau.edu

Siddharth S. Parida
Embry-Riddle Aeronautical University, PARIDAS@erau.edu

Using Machine Learning in Estimating Changing Bed Shear over a Flume Test Box

Ghada S. Ellithy, Ph.D., P.E., M.ASCE[1]; and Siddharth S. Parida, Ph.D.[2]

[1]Assistant Professor, Dept. of Civil Engineering, Embry-Riddle Aeronautical Univ., Daytona Beach, FL. Email: ellithyg@erau.edu
[2]Assistant Professor, Dept. of Civil Engineering, Embry-Riddle Aeronautical Univ., Daytona Beach, FL. Email: paridas@erau.edu

ABSTRACT

A dam or levee breach caused by overflow erosion is difficult to evaluate during an overtopping event due to difficulty in accessibility and quickly changing conditions. However, for assessment of risk associated with breach time and ensuing downstream consequences, the erosion rate of embankment soils during this process needs to be evaluated. Soil erosion and water depth measurements were taken during flume tests using a Shallow Water Lidar (SWL) system scans. The tests were conducted in a 1-m-wide tilting flume on three clean sand and gravel soil mixes with a median grain size D_{50} of 2, 5, and 20 mm. The box measured 0.45-m-wide $\times$ 1.2-m-long $\times$ 0.25-m-deep. Due to the confined environment of the flow in the flume, the acting bed shear changes with hydrodynamics of the flow differently from under a uniform flow. The scour hole generated in the test box reaches equilibrium when the acting bed shear is equal to the critical shear. Standard machine learning techniques were used to image soil and water profiles from noisy Lidar data. First, the data are filtered using zonal-averaging and then based on the filtered data; the methodology selects the best profiles from a competing set based on the minimum error each profile produces on the data. Once the profiles are obtained, erosion rates and bed shear are computed, and a qualitative assessment is carried out to understand the relationship between temporal and spatial dependence of erosion rate on bed shear and soil particle size. Erosion rate and shear stress reached their maximum value within the first 60–70 seconds of the test and spatially within 0.3 m from the upstream end of the test box. The erosion rate decreased by about 4 times from 0.13 cm/s to 0.03 cm/s as D_{50} increased from 2 mm to 20 mm at the same acting bed shear. The erosion rate for both mixes is reduced over time; however, the rate of reduction for D_{50} of 20 mm is much higher over the same test duration. The erosion rate was shown to be strongly correlated to the acting bed shear nonlinearly. The results indicate that the calculated spatial variation of shear stress over the duration of the tests is consistent with the formation of maximum depth of scour hole.

INTRODUCTION

The physical phenomenon of overflow erosion is complicated and is a function of the hydrodynamics of the hydraulic loading, the geomaterials that comprise the earthen structure as well as the geometry of the embankment. For flood risk assessment of water retaining structures such as dams and levees, the earthen structures are assumed to breach when they are overtopped. However, for a more accurate assessment and to estimate a realistic time and width of breach, more understanding of the erosion rate and mechanism is needed especially for coarse-grained (or non-cohesive) sand and gravel materials.

The response of a mix of coarse-grained material like sand and gravel and fine-grained material like clays to hydraulic loading is governed by the relative fractions of the cohesive and non-cohesive particles. Cohesive or fine-grained materials have been studied more in terms of overtopping erosion (Hanson and Simon 2001, Hanson et al. 2001), while uncertainty remains about the erosion parameters of coarse-grained materials. Erosion studies have been conducted in flumes where test boxes or small scale physical models are constructed and subjected to varying hydraulic loading to assess the erosion rate.

Measurements of the eroded soil surface are typically taken before and after the test after equilibrium is achieved. This does not give an accurate representation of the erosion process due to changing of flow conditions and pore water pressures within the soil. To have a better understanding of the erosion evolution during overflowing conditions, real-time measurements need to be taken. However, such measurements have previously been difficult due to accessibility, quickly changing conditions, and lack of technology. Moreover, the hydrodynamics of the flow and the formation of a scour hole within the test box present an additional challenge.

Meftah et al. 2020 studied the turbulence in the scour hole downstream of bed sills in non-cohesive sediments using Acoustic Doppler Velocimeter (ADV). They indicated that three flow velocity regions can be identified as shown in Figure 1: (i) region 1, where a free entering jet flows, originated by the flow condition over the box upstream edge; (ii) region 2, characterized by vortex formations (eddies) due to the jet diffusion, located near the bottom of the scour hole and extended along the upstream scour-side; and (iii) region 3, less turbulent and taking place downstream and outside the vortex region. Between regions 1 and 2, a hydraulic jump may occur, depending on the hydraulic conditions. In Figure 1, the arrows are indicative of the flow velocity at the different regions. The study while focusing at the scour depth at equilibrium, it did not provide measures of the erosion rate.
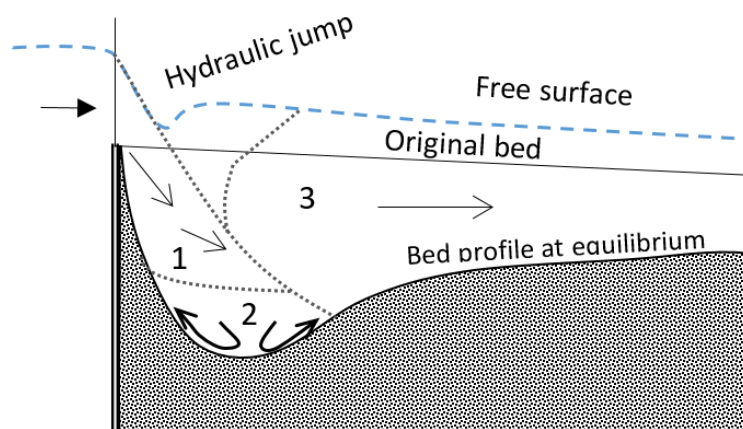
Figure 1. Definitional sketch of scour hole within the test box (after Meftah et al. 2020).

This paper presents the results from flume soil erosion tests performed on three sand and gravel soil mixes with median particle size D_{50} of 2, 5 and 20 mm. The testing conditions for the three mixes are almost similar which emphasizes the effect of D_{50} on the outcome results. A relatively new Lidar technology (Shallow Water Lidar, SWL) system was used to scan the test box and collect depth to soil and water surfaces under flowing conditions. In this study, scour and erosion data were collected during the evolution of the scour hole until equilibrium. This not only improve the prediction of erosion rate, but also help establish prediction of scour hole

formation in such soils in conditions where scour holes are formed around hydraulic structures like bridge piers, weirs and offshore platforms.

Machine learning has been used in the application of soil erosion on a regional scale; Mosavie et al 2020, Sahour et al. 2021. In this study, machine learning techniques were implemented to process the data to image soil profile and water surface. These modeled surfaces were used to estimate erosion rate and bed shear for each of the mixes.

MATERIAL PROPERTIES

Grain Size. The results presented from this study are for three clean sand and gravel mixes that maintain a D_{50} of about 2, 5 and 20 mm for the three mixes namely 1-1, 1-4, and 1-7, respectively and are shown in Figure 2. Pea gravel, 25 –mm (1-inch), and 75-mm (3 inch) minus gravel materials, and sands of different grain size distributions were mixed in different proportions to produce the three mixes. The gravel: sand percent are 34: 66, 50: 50 and 80:20 for mixes 1-1, 1-4 and 1-7, respectively. The uniformity coefficient: $C_u = D_{60}/D_{10}$, of the three mixes were greater than 6, and the curvature coefficient; $C_c = D_{30}/D_{10} \times D_{60}$, is between 1 and 3 for mixes 1-1 and 1-4, but less than 1 for mix 1-7. According to the unified soil classification system (USCS), mix 1-1 can be classified as well graded sand (SW), mix 1-4 as well graded gravel (GW), and mix 1-7 as poorly graded gravel (GP).
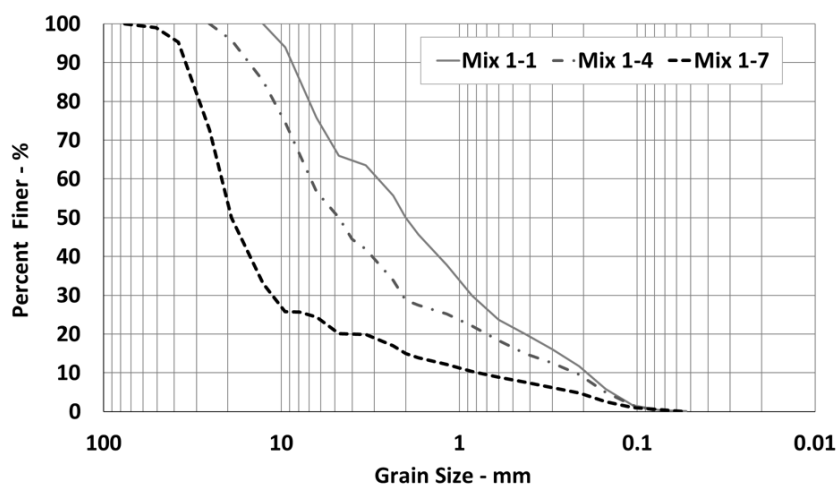
Figure 2. Grain size distribution for soil mixes 1-1, 1-4, and 1-7.

Density and Compaction. To prepare the three mixes, compaction was performed according to the standard Proctor test (ASTM D698-12) as shown in Figure 3 for mixes 1-1 and 1-4. For mix 1-7, and since more than 30% of the material is larger in size than 19 mm (3/4 inch), a special 30-cm (12 inch) diameter compaction mold was used to run a compaction test using the standard Proctor energy. The three mixes showed to be insensitive to the change in the moisture content as expected in sand and gravel soils. Mix 1-7 in particular showed to have free water content beyond 3%. For the evaluation of soil mixes erodibility, density conditions were selected near optimum as follows: water content; $w_c = 6\%$, 6%, and 3%, and dry density; $\gamma_d = 19.9, 18.8,$ and 20.4 kN/m^3 (127, 120, and 130 pcf) for mixes 1-1, 1-4, and 1-7, respectively, as indicated by the square marks in Figure 2 and summarized in Table 1.
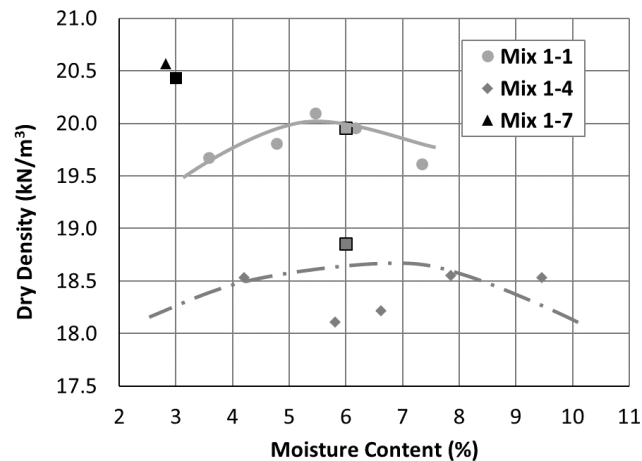
Figure 3. Compaction curves for soil mixes 1-1, 1-4, and 1-7 using standard Proctor test (ASTM D-698).

FLUME TESTING SETUP

The flume that was used in this study measured about 18.3 m (60 feet) in length, 0.91 m (3 feet) in width and 0.46 m (1.5 feet) in height. The flume bed could be tilted up to 8% (about 4.6 degrees) to achieve higher velocities at the same flow rate. A series of four variable-speed-pumps were used to adjust the flow rates in the flume. A flow ranging from 0.014 to 0.14 m³/sec (0.5- 5.0 cfs) was used in performing the erosion tests for this study.

The flow width of the flume was narrowed from 0.91 m to 0.46 m (1.5 feet) starting 3.0 m (10 feet) upstream from the test box. The test box was embedded in the flume bed and measured 1.22 m (4 feet) in length, 0.46 m (1.5 feet) in width and 0.18 m (7 inches) in depth. The soil sample was compacted in the box in two lifts, with calculated volume and weight to match the corresponding density and water content for each mix as mentioned above.

Before starting each test, the pumps were set to the selected flow level and the flume bed set to the target slope. The flow continued in each test until soil erosion was observed to have reached an almost equilibrium condition, where the erosion progress stopped or very slow erosion occurred. Prior to running the erosion tests, manual measurements of water depth with a sidewall mounted ruler and the velocity using a velocimeter were taken upstream and downstream of the test box. After the test is over and the water was stopped, measurements of the final soil surface were taken. A comparison of the SWL readings, manual readings and calculated values was made.

SHALLOW WATER LIDAR (SWL)

A Shallow Water Lidar (SWL) system (ASTRALiTe Inc.) was used to take measurements of the soil and water surfaces during the erosion test. The SWL system works by transmitting laser pulses from above the water and recording the time-delay between top and bottom reflections. Figure 4 shows how the SWL unit was mounted to a railing system on which the unit was traveling parallel and perpendicular to the flow direction. The SWL was oriented vertically with the laser beam normal to the horizontal. It was assumed that the angle of reflection of the laser

on the slopes that the flow was under will not affect the accuracy of the calculations. The railing system was about 0.75 m (2.5 feet) above the upper surface of the test box. An encoder was integrated in the railing system to measure horizontal position of the SWL parallel and perpendicular to the flow direction.
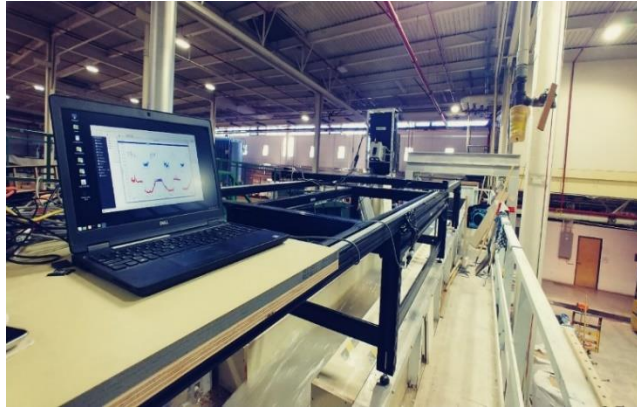
Figure 4. Shallow Water Lidar (SWL) system during performance.

The traveling speed averaged about 0.75 m/ sec with an average acceleration of 1.0 m/sec^2. A laptop was set up to enable monitoring of the real-time data from the Lidar system. The plots generated from the real-time data were available throughout the test. The SWL scans were performed on eight profiles along the test box (parallel to the direction of the flow) the eight profiles are 0.025 m (1 inch) apart and cover the middle 0.18 m (7 inch) of the test box width. The SWL scanned each single profile along the box length of 1.22 m (4 feet) in 3.5 seconds, and completed each loop in about 27.5 seconds. The SWL collected readings with a pulse rate of 8 kHz. More details could be found in Ellithy et al. 2017.

This raw surface data were post-processed by taking a mean value for a bin of 100 laser pulses to get an estimate of the distance to the soil surface. The data from the post-processing resulted in surface with ±1-cm vertical and horizontal precision. Prior to starting the erosion test, dry bed scans were taken by the SWL to be the datum of the scans taken during the test to calculate the erosion depth. Further calculations and data processing were performed using Matlab (MathWorks Inc. 2010).

Results and DISCUSSION

The SWL scanned both the water and soil surfaces during each test. For the tests discussed in this paper, the flow rate used was between 0.057 and 0.061 m^3/sec and the flume slope was 2% as summarized in Table 1.

Soil and water surface profiles. The mid-section (section 5) of the box was chosen to analyze erosion behavior of the soil. To understand erosion, one needs to first image the variation of soil and water surface with respect to time and space. The experimental data that was obtained from Lidar was used to this end. However, the data was very noisy which first needed to be cleaned up. To this end, a zonal-averaging algorithm was employed. The length of the box was split into 10 zones of 0.13m each. The water surface and soil surface height for each zone was chosen to be the average of respective water surface and soil surface height measured by the

Lidar in between these zones. Once the filtered water height and soil profile were obtained, non-linear regression was employed to image the evolution of the soil and water surfaces with respect to time using the Levenberg-Marquardt algorithm (Levenberg 1944). To choose the best model, a series of competing models were tested for each zone and the model which yielded the least R2 error was chosen. Such an approach for filtering and non-linear regression is quite common in the field of machine learning. The zoning ensures that the regression does not over-fit the noisy-data (Parida et al. 2019, 2020) and the model selection based on least R^2 error ensures that the best model is fitted to explain the data. With such a method in place, it was observed that most of the zones eroded exponentially and the rest almost linearly. Depending on the hydrodynamics of the flow and the soil mix that was being tested, it was seen that water surface fluctuates along with the evolution of the soil surface in a close pattern. From an erosion point of view, the absolute soil and water surfaces are irrelevant, but the difference between these i.e. the water depth is important since it is responsible for bed shear together with soil mix specific properties. Water depth was calculated by subtracting the modeled soil surface from the modeled water surface.

Table 1. Summary of soil mix properties and test conditions.

Mix/ D_{50} (mm)	Dry Density (kN/m^3)	Moisture content (%)	Flow Rate (m^3/sec)	Slope (%)	Initial Average Bed Shear (Pa)	Max Velocity, U_c (m/s)	Initial Erosion Rate (cm/s)
1-1/ 2	19.9	6	0.061	2	15.5	2.1	0.130
1-4/ 5	18.8	6	0.057	2	21.0	2.1	0.175
1-7/ 20	20.4	3	0.057	2	22.0	1.4	0.030

Figure 5 shows evolution of the water depth, with time, plotted against distance from the upstream end of the test box for the middle longitudinal section. Depending on the hydrodynamics of the flow and the soil mix particle size, the water surface fluctuates along with the evolution of the soil surface. In mix 4 (Figure 7b), it can be noted that the maximum water depth is in the zone between 0.2m-0.4m and this zone matches the observation of the location of maximum scour depth. Similar trends can be seen for the two other mixes.

Erosion Rate. Erosion rates shown in Figure 6 for the three mixes were calculated by dividing the difference in the soil surface by the elapsed time in between different time steps. As it could be noticed, the erosion rate is reduced significantly with time which is attributed to the developing of scour hole and the reduction in velocity and acting bed shear until equilibrium is achieved where no more erosion is occurring. The reduction in erosion rate increase with D_{50}. This reduction in erosion rate could not be calculated if the erosion measurements are not taken at small time intervals from the beginning of the test which was facilitated by the use of the SWL system.

The location of the highest erosion rate is within 0.13, and 0.4 m from upstream, and it moves towards the downstream side as the D_{50} increases. The maximum erosion rate when comparing mixes 1 and 7 decreases by about 4 times from 0.13 cm/s to 0.03 cm/s as D_{50} increases which is expected as the smaller particle size would be dislodged faster at the same acting bed shear. It is not only the D_{50} that increased but also the maximum particle size increased from about 12.5 mm (1/2 in) for mix 1 to 75 mm (3 in) for mix 7. During the test, it is noticed that the erosion rate of the two mixes is following the same trend as the initial as the erosion rate for both mixes is reduced over time, however, the rate of reduction for mix 7 is

much higher than that of mix over the same test duration. Briaud et al. 2008 reported test results and a chart for erosion rate versus bed shear for soils ranging between low to very high erodibility. The results presented in Table 1 are consistent with Briaud et al. 2008 chart qualitative classification of soils between medium to high erodibility. Also, the observation about the reduction of erosion rate as the D_{50} increases is in line with conclusions from previous similar experiments like, Hanson and Simon 2001, van Rijn 1984, van Rijn 1993, Visser et al. 1986, and Yalin 1977.
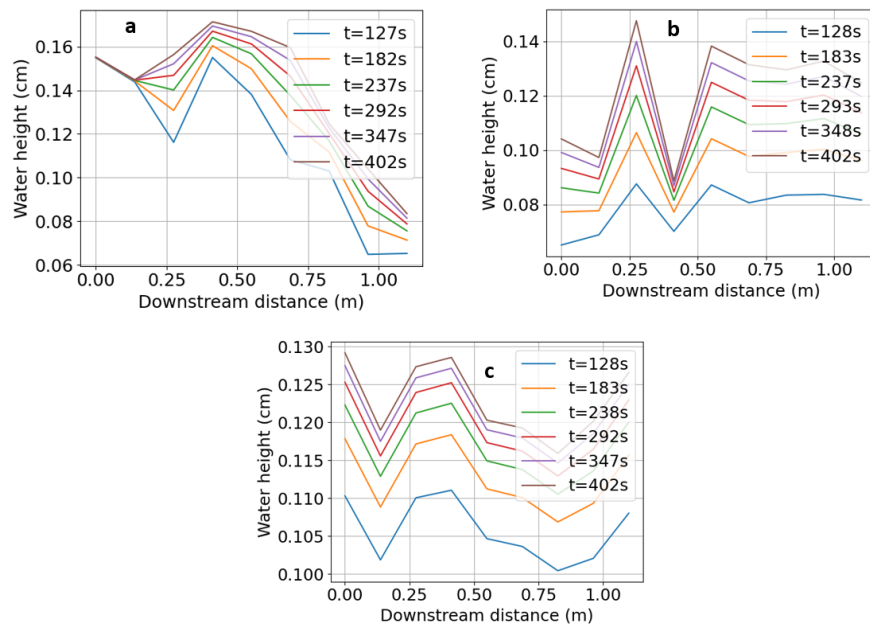
Figure 5. Evolution of water depth with time (a) mix 1-1, (b) mix 1-4, and (c) mix 1-7.
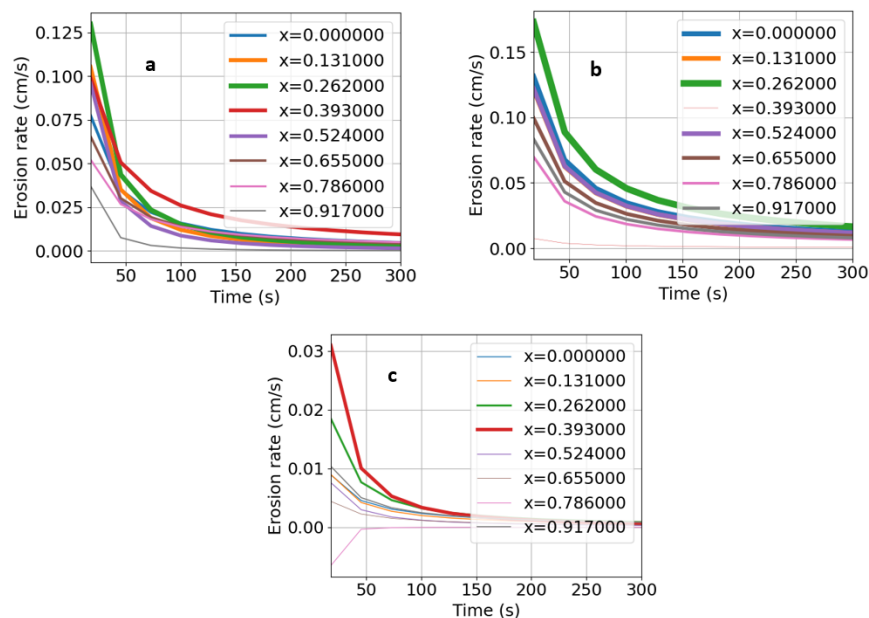
Figure 6. Erosion Rate with time. (a) mix 1-1, (b) mix 1-4, (c) mix 1-7.

The maximum initial erosion rate for mix 4 (D_{50}=5 mm) of 0.175 cm/s is larger than mix 1 (D_{50}=2 mm) of 0.13 cm/s could be explained by the fact that the gravel portion in mix 4 may have developed an equal mobility with the sand portion resulting in removal of larger portion of the soil mix. This phenomenon of equal mobility is a function of the grain size distribution and the acting bed shear. Similar observations have been made on other mixes tested under this study (but not presented in this paper).

Bed Shear. The following equation (Garcia, 2008) was used to estimate the bed shear τ acting at each bin. The velocity u is estimated given the water depth z at the given section by dividing the unit flow rate q (m³/s/m) by the water depth.

$$\frac{u}{u_*} = \frac{1}{\kappa} \ln(30 \frac{z}{k_s}) \tag{1}$$

where, u is the velocity (m/s), u_* is the shear velocity $= \sqrt{\frac{\tau}{\rho_w}}$ and ρ_w is the water density of 1,000 kg/m³, κ is von Karman's constant = 0.41, z is the water depth (difference between water and soil surface), k_s is a grain roughness coefficient varies between D_{50} and 3.0 D_{90}.

Figure 7 shows the changes in soil surface, calculated velocity and shear stress over the test box longitudinal section and over time for mix 4. Figure 7a shows that the bottom of the scour hole is within 0.2 to 0.4 m, Figure 7c indicates that the highest shear and lowest shear areas are between 0.0 to 0.2 m and 0.2 and 0.4 m, respectively. These two areas are the ones leading to and within the maximum scour depth. This observation is consistent with findings of Meftah et al. 2020 who indicated that the jet-flow of region 1 in Figure 1 (0.0 to 0.2 m) controls the scour hole development. This is due to its high impinging velocity and consequently acting shear, which leads to an increase of the flow erosive action on the soil bed. As the jet size increases over time, the jet gradually loses its erosive potential which is indicated by the reduction in shear stress over time. The state of equilibrium occurs when the path of the impinging jet becomes sufficiently long and its diffused velocity is reduced to values lower than the minimum value required for sediment movement and the acting bed shear becomes lower than the critical shear.
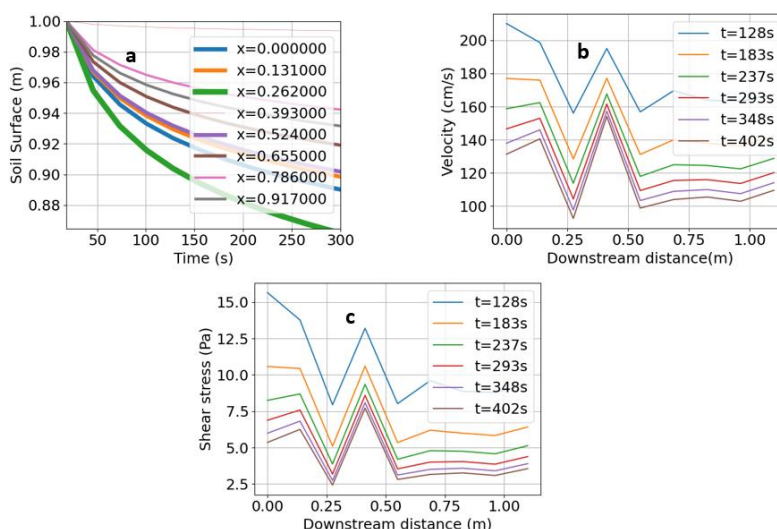
Figure 7. Changes in soil surface, velocity and shear stress for mix 4 over distance and time. (a) soil surface, (b) velocity (cm/s), (c) shear stress (Pa).

In the region 2 in Figure 1 (0.2m to 0.4 m), a significant reduction of the flow velocity occurs, due to turbulence and formation of eddies, starting at the position of maximum scour depth and extending towards the upstream test box edge, forming a sort of clockwise local vortex. Then, another portion of increased velocity occurs that shifts the flow downstream, from the position of the maximum scour depth.
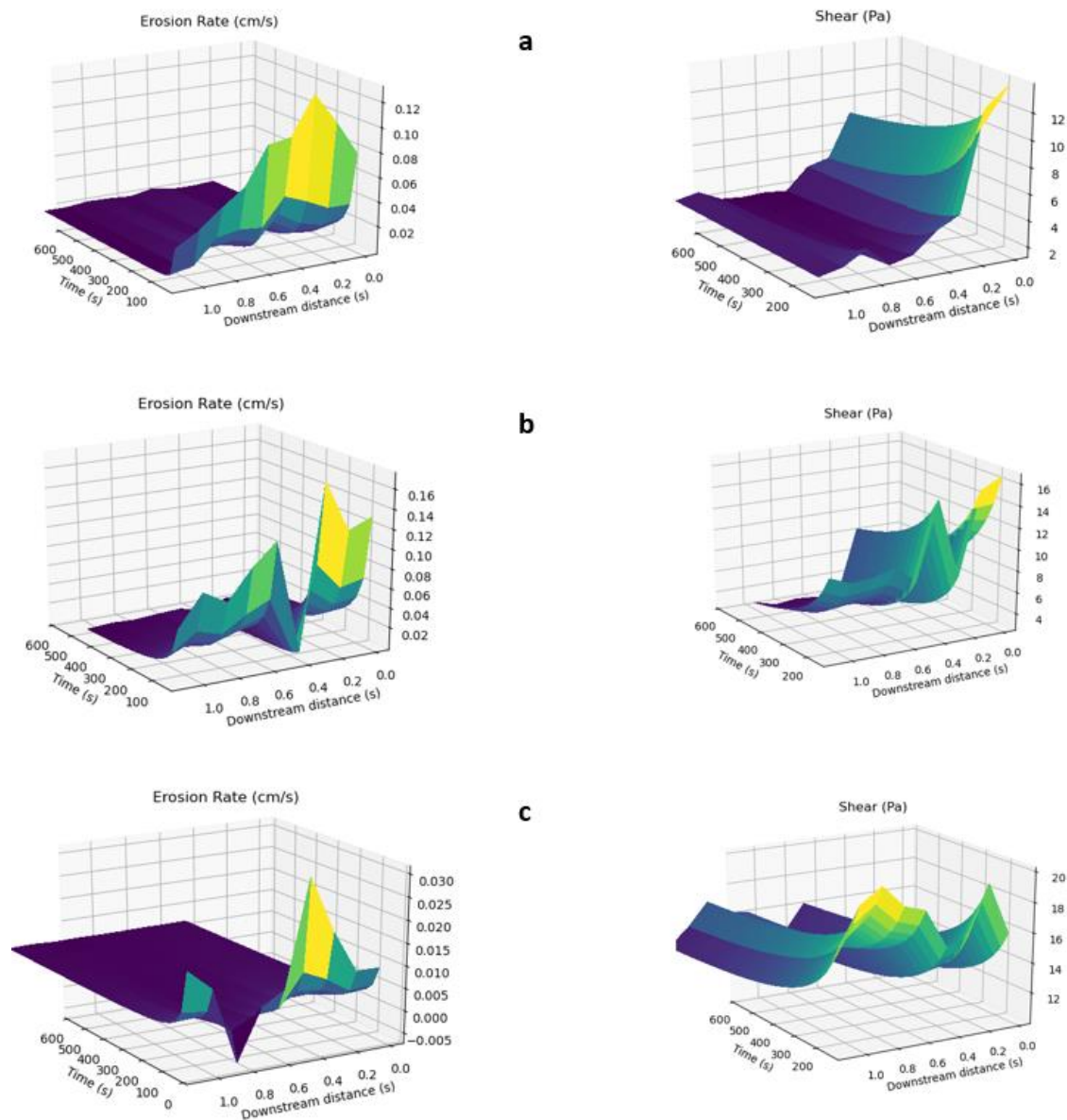
Figure 8. Variation of erosion rate and shear stress with respect to space and time. (a) mix 1, (b) mix 4, (c) mix 7

Erosion Rate and Bed Shear Relationship. Figure 8 shows the spatial and temporal variation of the erosion rate and shear stress for the three mixes. It is observed that there is a strong correlation between the erosion rate and shear stress both in time and space. For an example, for mix 1, both erosion rate and shear stress reach their maximum value within the first

60 to 70 seconds and spatially within 0.3 m from the upstream end of the test box. It can also be observed that both erosion rate and shear stress decay similarly with time and space. This strong correlation is attributed to the erosion of soil profile and accumulation of water which reduces the velocity and hence the shear stress and corresponding erosion rate.

Similar trend could be observed for mixes 4 and 7, but due to the different D_{50} and maximum size values of the three mixes, the relationship between the erosion rate and shear stress is not exact. However, from these plots, it can be clearly argued that the erosion rate is a nonlinear function of the temporal and spatial variation of shear stress and the particle size. Similar conclusions were shown in Ellithy et al. 2018a, b.

SUMMARY AND CONCLUSIONS

This paper summarizes the results from flume erosion tests on three sand and gravel soil mixes with median grain size D_{50} of 2, 5 and 20 mm. The results demonstrate the advantage of implementing machine learning techniques on real-time data obtained by a shallow-water Lidar (SWL) system in scanning erosion process and scour hole progression in flume experiments. The SWL provides the ability to measure the water and soil surfaces erosion in real time with flowing water even under turbulent conditions. This enables the calculation of bed shear acting along the scour hole. The SWL provided high-precision longitudinal profiles of the test box of about 1-cm horizontal and vertical resolution over a 1.22 m (4 feet) span under flowing conditions up to 0.061m^3/sec.

The results presented in this paper indicate that the erosion rate significantly decreases with time from an initial high value. This change over the duration of the test could not be detected if the erosion measurements are not taken at small time intervals which was facilitated by the use of the SWL system. The erosion rate was shown to be strongly correlated to the acting bed shear nonlinearly. The bed shear temporal and spatial variation was calculated using the soil and water profile images as were obtained by processing the SWL data using machine learning techniques. This ensured careful nonlinear regression by not overfitting on noisy data.

The initial erosion rate and the level of reduction over time is affected by the maximum and median particle size D_{50}. Erosion rate and shear stress were found to reach their maximum value within the first 60 to 70 seconds of the test. The erosion rate decreases by about 4 times from 0.13 cm/s to 0.03 cm/s as D_{50} increases from 2 mm to 20 mm at the same acting bed shear. The erosion rate for both mixes is reduced over time, however, the rate of reduction for D_{50} of 20 mm is much higher over the same test duration.

The results indicate that the calculated spatial variation of shear stress over the duration of the tests is consistent with the formation of maximum depth of scour hole. The maximum shear stress was calculated along the jet-flow region of high impinging velocity which leads to an increase in erosive action followed by a significant reduction of the flow velocity and shear at the maximum scour depth due to turbulence and formation of eddies.

ACKNOWLEDGEMENT

REFERENCES

ASTM. (2012). *Standard test method for Laboratory Characteristics of Soil Using Standard Effort (12,400 ft-lbf/ft³ (600 kN-m/m³)*. American Society for Testing and Materials Standard Designation D 698-12, West Conshohocken, PA.

ASTRALiTe. *Atmospheric & Space Technology Research Associates*, LLC. www.astralite.net.

Briaud, J. L., Chen, H. C., Covindasamy, A. V., and Storesund, R. (2008). "Levee erosion by overtopping in New Orleans during the Katrina hurricane". *JGGE* Vol. 134, No. 5, May 1.

Ellithy, G. S., Wibowo, J. L., and Corcoran, M. K. (2018). "Erosion Rate Equations for Coarse-Grained Materials Using a Small Flume Testing", of the *9th International Scour and Erosion (ICSE 2018)*, Taipei, Taiwan, November 5–8, 2018, 113. London, UK: CRC Press/Balkema.

Ellithy, G. S., Wibowo, J. L., and Corcoran, M. K. (2018). "Determination of Erosion Parameters of Coarse- Grained Materials Using a Small Flume", *Protections 2018 Conf Pro.*, UK.

Ellithy, G. S., Savant, G., and Wibowo, J. L. (2017). *Effect of Soil Mix on Overtopping Erosion*, ASCE EWRI, Sacramento, CA 21-25 May.

Garcia, H. (2008). Sedimentation Engineering, ASCE Manuals and Reports on Engineering Practice No. 110.

Hanson, G. J., and Simon, A. (2001). "Erodibility of cohesive streambeds in the loess area of the Midwestern, USA". *Hydrological Processes*, p 23-38.

Hanson, G. J., Robinson, K. M., and Cook, K. R. (2001). "Prediction of headcut migration using a deterministic approach," *Transaction of the ASAE*, 44(3), 525-531.

Levenberg, K. (1944). "A Method for the Solution of Certain Non-Linear Problems in Least Squares". *Quarterly of Applied Mathematics*. 2 (2): 164–168. doi:

MathWorks, Inc. (2010). *MATLAB version 7.10.0*. Natick, Massachusetts.

Meftah, M., De Serio, F., De Padova, D., and Mossa, M. (2020). "Hydrodynamic structure with scour hole downstream of bed sills". *Water* 2020, 186.

Mosavi, A., Hosseini, F. S., Choubin, B., Taromideh, F., Rahi, C., and Dineva, A. A. (2020). "Susceptibility Mapping of Soil Water Erosion Using Machine Learning Models". *Water* 2020, 12.

Parida, S. S., Nikellis, A., Sett, K., and Singla, P. (2020). Model-data fusion for seismic performance evaluation of an instrumented highway bridge, *Earthquake Engng Struct Dyn.*; 49: 1559–1578.

Parida, S. S., Sett, K., and Singla, P. (2019). Model-data fusion for spatial and statistical characterization of soil parameters from geophysical measurements, *Soil Dynamics and Earthquake Engineering*, Volume 124, Pages 35-57, ISSN 0267-7261,

Sahour, H., Gholami, V., Vazifendan, M., and Saeedi, S. (2021). *Machine learning applications for water-induced soil erosion modeling and mapping*. Elsevier,

van Rijn, L. C. (1984). "Sediment pick-up functions." *Journal of Hydraulic Engineering* 110(10), 1494-1502.

van Rijn, L. C. (1993). *Principle of sediment transport in rivers, estuaries, coastal seas*. Aqua Publications, Amsterdam, The Netherlands.

Yalin, M. S. (1977). *Mechanics of sediment transport*. Pergamon Press, Oxford, England.